Supplementary information for

Black carbon aerosols in China: Spatial-temporal variations and lessons from long-term atmospheric observations

Huang Zheng [1], Shaofei Kong [2], Deping Ding [3, 4], MarjanSavadkoohi [5, 6], Congbo Song [7], Mingming Zheng [8], Roy M. Harrison [9, 10]

[1] College of Resource and Environmental Engineering, Wuhan University of Science and Technology, 430081 Wuhan, China

[2] Department of Atmospheric Sciences, School of Environmental Studies, China University of Geosciences, Wuhan, 430078, China

[3] Beijing Weather Modification Center, Beijing, 100089, China

[4] Beijing Key Laboratory of Cloud, Precipitation and Atmospheric Water Resources, Beijing, 100089, China

[5] Institute of Environmental Assessment and Water Research (IDAEA-CSIC), 08034, Barcelona, Spain

[6] Department of Mining, Industrial and ICT Engineering (EMIT), Manresa School of Engineering (EPSEM), Universitat Politécnica de Catalunya (UPC), Manresa, 08242, Spain

[7] National Centre for Atmospheric Science (NCAS), Department of Earth and Environmental Science, The University of Manchester, Manchester M13 9PL, U.K.

[8] School of Chemical and Environmental Engineering, Wuhan Polytechnic University, Wuhan, 430023, China

[9] School of Geography, Earth and Environment Sciences, University of Birmingham, Birmingham B15 2TT, U.K.

[10] Department of Environmental Sciences, Faculty of Meteorology, Environment and Arid Land Agriculture, King Abdulaziz University, PO Box 80203, Jeddah, Saudi Arabia

Correspondence: Shaofei Kong (kongshaofei@cug.edu.cn) and Deping Ding (zytddp@vip.sina.com)

Text S1 Reprocessing of ground observations from previous studies and observations.

In this study, data from 2015 and 2017 were collected from different sources, including published papers, observation networks, and publicly accessible websites. For each data source, different processing methods were applied, as described in detail below.

For data collected from EBAS, the light absorption coefficients (b_{abs}) were converted into eBC mass concentrations using the instrument-specific mass absorption cross-section (MAC). The light absorption coefficients from EBAS were obtained from several instruments, including MAAP-5012, CLAP-10, PASS-3, and Aethalometers (AE16, AE31, AE33, and AE42). For MAAP-5012, CLAP-10, and PASS-3, a MAC value of 6.6 $m^2\ g^{-1}$ at 637 nm was used, and it was adjusted for other wavelengths as determined by the instruments. For AE16, AE31, and AE42, a MAC value of 16.6 $m^2\ g^{-1}$ at 880 nm was used to convert babs at 880 nm into eBC mass concentrations. For AE33, a MAC value of 7.77 $m^2\ g^{-1}$ at 880 nm was used.

To calculate station-specific AAE, b_{abs} measured by the Aethalometer (AE42, AE31, and AE33) were used. Specifically, b_{abs} at 370 nm and 880 nm were used to calculate the AAE value ($AAE = \log(b_{abs\_370} / b_{abs\_880}) / \log(880 / 370)$). Similarly, eBC sources were apportioned using the default AAE combination ($AAE_{lf} = 1.0$ and $AAE_{sf} = 2.0$) and wavelengths of 370 nm and 880 nm.

For data collected from the US EPA, the annual mean value for "Black carbon at 880 nm" was used and reported as eBC concentrations. Additionally, the “UV carbon at 370 nm” along with "Black carbon at 880 nm" were used to calculate AAE and apportion eBC sources. Specifically, “UV carbon at 370 nm” and "Black carbon at 880 nm" were converted into babs at 370 nm and 880 nm by multiplying by 39.5 $m^2\ g^{-1}$ and 16.6 $m^2\ g^{-1}$, respectively. The AAE calculation and BC source apportionment were conducted as discussed for EBAS data.

For data collected from UK AIR, the eBC mass concentration at 880 nm and “UVBC” were used. The babs at 370 nm were calculated as 39.5*(BC + UVBC). The methods for calculating AAE and BC source apportionment were as described above. To ensure robust results, a data availability threshold of 50% was applied to data collected from EBAS, US EPA, and UK AIR.

For data collected from published papers, if eBC source apportionment results were reported, the AAE value was derived from these results. A cross-check between this method and the AAE calculated as the ratio of babs at two wavelengths showed an uncertainty of approximately 5%.

To calculate the trends of BC from different sources, the annual values were used, and the slope was calculated using the Theil-Sen method, consistent with the data processing in this study. For trends reported by previous studies, we only selected papers that used the Theil-Sen method.

Table S1 Details information of black carbon monitoring station in this study.

Code	Site name	Type [a]	Lon	Lat	MAC (m^2 g^{-1}) [b]	Instrument
51058	Akadala	B	87.97	47.10	8.9	AE31
51462	Urumqi	U	87.56	43.85	8.9	AE31
51747	Tzhong	RU	83.67	39.00	8.9	AE31
52203	Hami	RU	93.52	42.82	8.9	AE31
52267	Ejilaqi	RU	101.07	41.95	8.9	AE31
52418	Dunhuang	RU	94.68	40.15	8.9	AE31
52859	Waliguan	B	100.62	36.27	14	AE31&AE33
53276	Zhurihe	RU	112.90	42.40	11.2	AE31
53646	Yulin	RU	109.78	38.27	7.3	AE31
53787	Yushe	RU	112.98	37.07	12.3	AE31
54084	Longfengshan	B	127.60	44.73	14.4	AE31
54102	Xilinhaote	RU	116.12	43.95	11.2	AE31
54135	Tongliao	RU	122.27	43.60	14.4	AE31
54161	Changchun	U	125.22	43.90	14.4	AE31
54339	Anshan	U	123.00	41.08	14.4	AE31
54342	Shenyang	U	123.52	41.73	14.4	AE31
54346	Benxi	U	123.78	41.32	14.4	AE31
54351	Fushun	U	124.08	41.92	14.4	AE31
54421	Shangdianzi	B	117.12	40.65	11.2	AE31 &AE33
54511	Guanxiangtai	U	116.47	39.80	11.2	AE31
54662	Dalian	U	121.63	38.90	14.4	AE31
54725	Huimin	RU	117.53	37.48	11.2	AE31
55591	Lasa	U	91.13	29.67	8.8	AE31
56294	Chengdu	U	103.83	30.70	14.1	AE31
56449	Shangri−L	B	99.70	27.83	14	AE31&AE33
57083	Zhengzhou	U	113.65	34.72	12.3	AE31
57131	Xi'an	U	108.97	34.43	9.4	AE31
57278	Xiangfan	U	112.17	32.03	14	AE31
57461	Yichang	U	111.30	30.70	14	AE31
57494	Wuhan	U	114.13	30.62	10.2	AE31
57596	Jinsha	B	114.20	29.63	12.3	AE31&AE33
57957	Guilin	RU	110.30	25.32	13.4	AE31
58215	Shouxian	RU	116.78	32.55	14	AE31
58363	Dongtan	RU	122.00	31.50	12.3	AE31
58370	Pudong	U	121.55	31.22	14	AE31
58448	Lin'an	B	119.73	30.30	12.3	AE31&AE33
58457	Hangzhou	U	120.17	30.23	14	AE31
58477	Dinghai	RU	122.10	30.03	14	AE31
58506	Lushan	RU	115.98	29.58	12.3	AE31
58659	Wenzhou	U	120.65	28.03	14	AE31
58665	Hongjia	U	121.42	28.62	14	AE31

Code	Site name	Type [a]	Lon	Lat	MAC (m^2 g^{-1}) [b]	Instrument
59287	Guangzhou	U	113.33	23.17	14	AE31
59289	Dongguan	U	113.73	22.97	8.8	AE31
59431	Nanning	U	108.22	22.63	13.4	AE31
59481	Panyu	RU	113.32	22.93	8.8	AE31
59493	Shenzhen	U	114.00	22.53	8.8	AE31
G3101	Haizhu	U	113.34	23.07	8.8	AE31
K9400	Lishui	U	119.92	28.45	14	AE31
W3467	Gaolan	RU	103.93	36.35	7.3	AE31
Z9736	Changde	RU	111.68	29.05	18	AE31

[a] B: Baseline station; RU: Rural station; U: Urban station.

[b] MAC: Mass absorption across section. The station-specific MAC value at 880 nm (for AE31) is from Guo et al. (2020) except Wuhan, which is from Zheng et al. (2021).

Table S2 Station specific (SS) AAE values derived from frequency distributions and BC source apportionment results (mean ± standard deviation) derived from station specific AAE values and default AAE combination (AAE_{lf} = 1.0 and AAE_{sf} = 2.0) and their changes (defined as the differences between SS AAE and default AAE).

Code	SS AAE		eBC_{lf} (%)			eBC_{sf} (%)		
	AAE_{lf}	AAE_{sf}	SS AAE	Default	Delta	SS AAE	Default	Delta
51462	1.02	1.70	54.2 ± 23.1	70 ± 16.3	−22.6	45.8 ± 23.1	30.0 ± 16.3	52.7
51747	0.89	2.53	66.5 ± 24.9	49.7 ± 32.4	33.8	33.5 ± 24.9	50.3 ± 32.4	−33.4
52203	1.00	2.22	57.2 ± 26.4	46.5 ± 29.2	23.0	42.8 ± 26.4	53.5 ± 29.2	−20.0
53276	0.79	2.09	52.5 ± 23.3	53.6 ± 27.5	−2.10	47.5 ± 23.3	46.4 ± 27.5	2.40
53787	0.75	1.68	50.0 ± 24.2	76.4 ± 20.0	−34.6	50.0 ± 24.2	23.6 ± 20.0	112
54084	0.91	1.79	45.6 ± 24.0	61.9 ± 21.6	−26.3	54.4 ± 24	38.1 ± 21.6	42.8
54102	0.91	1.92	57.0 ± 25.5	64.2 ± 25.5	−11.2	43.0 ± 25.5	35.8 ± 25.5	20.1
54161	0.90	1.61	36.4 ± 26.1	65.5 ± 21.8	−44.4	63.6 ± 26.1	34.5 ± 21.8	84.3
54339	0.87	1.89	47.7 ± 28.7	57.9 ± 29.0	−17.6	52.3 ± 28.7	42.1 ± 29.0	24.2
54342	0.90	1.61	44.4 ± 25.6	72.1 ± 18.9	−38.4	55.6 ± 25.6	27.9 ± 18.9	99.3
54346	0.89	1.58	41.2 ± 25.9	72.4 ± 18.2	−43.1	58.8 ± 25.9	27.6 ± 18.2	113
54351	0.89	1.63	44.7 ± 22.0	72.1 ± 16.0	−38.0	55.3 ± 22.0	27.9 ± 16.0	98.2
54421	0.86	1.74	45.7 ± 27.8	66.6 ± 24.2	−31.4	54.3 ± 27.8	33.4 ± 24.2	62.6
54725	0.90	1.81	44.5 ± 24.8	59.4 ± 24.1	−25.1	55.5 ± 24.8	40.6 ± 24.1	36.7
55591	0.91	1.70	54.2 ± 25.5	73.8 ± 20.6	−26.6	45.8 ± 25.5	26.2 ± 20.6	74.8
56449	0.93	1.88	51.2 ± 32.8	58.9 ± 32.5	−13.1	48.8 ± 32.8	41.1 ± 32.5	18.7
57083	0.83	1.54	53.8 ± 23.2	84.1 ± 13.7	−36.0	46.2 ± 23.2	15.9 ± 13.7	191
57131	0.87	1.64	52.4 ± 23.1	77.1 ± 17.4	−32.0	47.6 ± 23.1	22.9 ± 17.4	108
57278	0.92	1.64	59.2 ± 20.7	80.3 ± 12.9	−26.3	40.8 ± 20.7	19.7 ± 12.9	107
57494	0.94	1.60	46.2 ± 28.3	71.1 ± 22.3	−35.0	53.8 ± 28.3	28.9 ± 22.3	86.2
58215	0.96	1.57	58.8 ± 21.0	81.5 ± 11.5	−27.9	41.2 ± 21.0	18.5 ± 11.5	123
58370	0.98	1.69	55.4 ± 25.0	71.5 ± 21.3	−22.5	44.6 ± 25.0	28.5 ± 21.3	56.5
58448	0.92	1.56	34.8 ± 24.8	67.1 ± 21.3	−48.1	65.2 ± 24.8	32.9 ± 21.3	98.2
58457	0.89	1.45	60.5 ± 21.1	89.5 ± 9.3	−32.4	39.5 ± 21.1	10.5 ± 9.30	276
58477	0.87	1.51	56.4 ± 22.9	85.8 ± 12.4	−34.3	43.6 ± 22.9	14.2 ± 12.4	207
58506	0.84	1.71	48.9 ± 26.8	70.4 ± 24.8	−30.5	51.1 ± 26.8	29.6 ± 24.8	72.6
58665	0.94	1.58	60.4 ± 21.8	82.3 ± 14.2	−26.6	39.6 ± 21.8	17.7 ± 14.2	124
59289	0.89	1.58	56.1 ± 27.6	79.8 ± 20.8	−29.7	43.9 ± 27.6	20.2 ± 20.8	117
59431	0.94	1.56	47.0 ± 20.1	75.7 ± 13.1	−37.9	53.0 ± 20.1	24.3 ± 13.1	118
59481	0.98	1.52	52.5 ± 17.3	80.0 ± 8.50	−34.4	47.5 ± 17.3	20.0 ± 8.50	138
59493	0.88	1.43	52.3 ± 20.2	87.1 ± 10.7	−40.0	47.7 ± 20.2	12.9 ± 10.7	270
G3101	0.93	1.51	62.7 ± 20.5	87.1 ± 9.70	−28.0	37.3 ± 20.5	12.9 ± 9.70	189
K9400	0.89	1.53	52.6 ± 22.2	82.1 ± 12.2	−35.9	47.4 ± 22.2	17.9 ± 12.2	165
W3467	1.00	1.74	55.5 ± 22.1	69.8 ± 16.2	−20.5	44.5 ± 22.1	30.2 ± 16.2	47.4

Table S3 Hyperparameter tunning results for RF model used to normalize the influence of weather on black carbon and its source.

Code	min.node.size			mtry			num.trees		
	eBC	eBC_{lf}	eBC_{sf}	eBC	eBC_{lf}	eBC_{sf}	eBC	eBC_{lf}	eBC_{sf}
52203	1	4	3	11	7	9	754	694	457
52418	6	3	1	13	9	11	436	536	348
53276	1	1	1	7	7	6	980	980	495
53787	4	1	4	7	6	9	903	505	921
54084	4	3	4	9	9	9	549	536	549
54102	8	2	10	5	4	8	483	428	123
54161	1	2	5	12	12	8	480	813	359
54339	3	1	1	6	6	10	500	139	760
54342	4	5	2	7	7	8	195	468	235
54346	4	6	4	9	9	9	415	149	415
54351	1	2	2	10	7	7	687	432	621
54421	1	4	2	5	4	7	146	573	621
54511	1	6	1	11	10	12	675	822	751
54662	4	4	4	9	9	7	921	921	903
54725	1	2	1	10	11	7	825	408	133
56294	2	1	2	12	10	11	533	610	817
56449	2	3	2	13	13	13	437	244	437
57083	4	2	4	10	8	9	852	208	905
57131	4	1	5	10	11	12	606	675	585
58448	1	2	2	7	8	8	980	814	814
58506	4	5	2	13	9	5	585	235	375
59431	2	2	2	6	6	6	773	773	773
59481	4	5	6	9	6	8	549	848	370
59493	2	4	1	7	6	11	374	777	887
W3467	7	1	5	8	11	9	694	826	311

Table S4 The surface BC concentrations derived from different CMIP6 historical simulations and other models.

Model name	Institution, country	Ensembles	Resolution	Experiment	Variables
CESM2-WACCM	NCAR, USA	1	100 km	Historical	mmrbc
CNRM-ESM2-1	CNRM-CERFACS, France	2	250 km	Historical	mmrbc
GFDL-ESM4	NOAA-GFDL, USA	1	100 km	Historical	mmrbc
GISS-E2-1-G-CC	NASA-GISS/USA	5	250 km	Historical	mmrbc
MRI-ESM2-0	MRI/Japan	6	100 km	Historical	mmrbc
UKESM1-0-LL	NIWA, MOHC, NIMS-KMA	3	250 km	Historical	mmrbc
MERRA2	NOAA, USA	—	0.625˚ × 0.5˚	−	BCSMASS
TAP	Tsinghua, China	—	10 km	−	BC

Table S5 Statistics (mean ± standard deviation, 5th, and 95th percentiles) of black carbon concentrations (eBC), BC from liquid fuel (eBC_{lf}) and solid fuel (eBC_{sf}) combustion, and AAE values in each station.

Code	eBC (μg m^{-3})		eBC_{lf} (μg m^{-3})		eBC_{sf} (μg m^{-3})		AAE_{370_950}	
	Mean ± SD	[5th, 95th]	Mean ± SD	[5th, 95th]	Mean ± SD	[5th, 95th]	Mean ± SD	[5th, 95th]
51462	1.69 ± 1.53	[0.31, 4.81]	0.89 ± 0.81	[0.03, 2.42]	0.80 ± 0.95	[0.09, 2.83]	1.37 ± 0.20	[1.11, 1.70]
51747	0.80 ± 0.89	[0.18, 2.08]	0.55 ± 0.66	[0.00, 1.52]	0.25 ± 0.40	[0.03, 0.76]	1.60 ± 0.45	[1.04, 2.38]
52203	2.09 ± 2.57	[0.27, 7.39]	1.03 ± 1.34	[0.00, 3.57]	1.07 ± 1.72	[0.04, 4.67]	1.66 ± 0.40	[1.09, 2.37]
53276	0.50 ± 0.56	[0.10, 1.41]	0.26 ± 0.32	[0.00, 0.79]	0.23 ± 0.34	[0.03, 0.75]	1.56 ± 0.35	[1.04, 2.16]
53787	2.07 ± 1.35	[0.49, 4.59]	1.12 ± 0.98	[0.03, 2.89]	0.96 ± 0.76	[0.20, 2.47]	1.27 ± 0.27	[0.91, 1.70]
54084	0.67 ± 0.75	[0.11, 1.98]	0.27 ± 0.35	[0.00, 0.84]	0.39 ± 0.52	[0.03, 1.25]	1.53 ± 0.30	[1.04, 2.04]
54102	0.11 ± 0.12	[0.02, 0.30]	0.07 ± 0.08	[0.00, 0.21]	0.04 ± 0.06	[0.00, 0.12]	1.41 ± 0.32	[0.98, 1.95]
54161	2.63 ± 2.76	[0.39, 7.78]	1.00 ± 1.54	[0.00, 3.63]	1.62 ± 1.70	[0.15, 4.91]	1.45 ± 0.29	[1.01, 1.96]
54339	1.36 ± 1.10	[0.36, 3.40]	0.71 ± 0.71	[0.00, 2.03]	0.66 ± 0.64	[0.08, 1.95]	1.55 ± 0.43	[0.93, 2.31]
54342	6.67 ± 6.52	[0.73, 20.4]	3.12 ± 3.65	[0.00, 10.3]	3.54 ± 3.88	[0.34, 12.0]	1.36 ± 0.26	[1.00, 1.79]
54346	4.95 ± 4.31	[0.76, 13.8]	2.01 ± 2.25	[0.00, 6.51]	2.94 ± 2.90	[0.27, 8.81]	1.37 ± 0.23	[1.02, 1.75]
54351	2.22 ± 1.87	[0.43, 5.88]	0.99 ± 0.97	[0.01, 2.81]	1.23 ± 1.18	[0.17, 3.49]	1.38 ± 0.21	[1.04, 1.72]
54421	1.30 ± 1.30	[0.15, 3.96]	0.63 ± 0.77	[0.00, 2.03]	0.68 ± 0.85	[0.08, 2.46]	1.38 ± 0.31	[0.96, 1.86]
54725	1.31 ± 1.35	[0.26, 3.95]	0.61 ± 0.69	[0.00, 1.89]	0.70 ± 0.82	[0.10, 2.29]	1.46 ± 0.29	[1.06, 1.90]
55591	2.24 ± 2.74	[0.42, 6.88]	1.20 ± 1.41	[0.00, 3.76]	1.04 ± 1.82	[0.14, 3.64]	1.31 ± 0.26	[1.01, 1.77]
56449	0.16 ± 0.12	[0.03, 0.40]	0.10 ± 0.11	[0.00, 0.31]	0.06 ± 0.06	[0.00, 0.17]	1.38 ± 0.37	[0.94, 2.10]
57083	4.58 ± 5.39	[0.56, 15.5]	2.50 ± 3.49	[0.13, 8.82]	2.08 ± 2.74	[0.17, 7.45]	1.19 ± 0.20	[0.91, 1.51]
57131	4.75 ± 7.19	[0.25, 20.7]	2.96 ± 4.87	[0.01, 13.26]	1.78 ± 2.80	[0.14, 8.13]	1.29 ± 0.21	[1.01, 1.67]
57278	1.90 ± 1.40	[0.37, 4.78]	1.13 ± 0.93	[0.13, 3.06]	0.76 ± 0.70	[0.08, 2.13]	1.27 ± 0.18	[1.01, 1.57]
57494	5.26 ± 4.42	[0.97, 14.2]	2.73 ± 3.21	[0.00, 9.09]	2.53 ± 2.27	[0.27, 7.07]	1.25 ± 0.21	[0.98, 1.62]
58215	1.52 ± 1.16	[0.38, 3.87]	0.87 ± 0.75	[0.14, 2.34]	0.65 ± 0.69	[0.08, 1.96]	1.26 ± 0.18	[1.02, 1.57]
58370	1.31 ± 1.04	[0.32, 3.37]	0.82 ± 0.80	[0.00, 2.35]	0.49 ± 0.36	[0.09, 1.21]	1.31 ± 0.24	[1.04, 1.68]
58448	1.79 ± 1.15	[0.49, 4.02]	0.71 ± 0.79	[0.00, 2.17]	1.08 ± 0.67	[0.24, 2.38]	1.30 ± 0.16	[1.07, 1.57]
58457	1.71 ± 1.18	[0.45, 4.07]	1.11 ± 1.01	[0.13, 3.06]	0.60 ± 0.43	[0.11, 1.48]	1.11 ± 0.13	[0.93, 1.36]
58477	0.82 ± 0.65	[0.16, 2.11]	0.47 ± 0.43	[0.04, 1.33]	0.35 ± 0.35	[0.04, 1.06]	1.19 ± 0.18	[0.94, 1.51]
58506	0.60 ± 0.51	[0.07, 1.56]	0.33 ± 0.36	[0.00, 1.00]	0.27 ± 0.24	[0.03, 0.73]	1.30 ± 0.28	[0.94, 1.76]

Code	eBC (μg m^{-3})		eBC_{lf} (μg m^{-3})		eBC_{sf} (μg m^{-3})		AAE_{370_950}	
	Mean ± SD	[5^{th}, 95^{th}]	Mean ± SD	[5^{th}, 95^{th}]	Mean ± SD	[5^{th}, 95^{th}]	Mean ± SD	[5^{th}, 95^{th}]
58665	1.56 ± 1.11	[0.38, 3.77]	0.98 ± 0.79	[0.09, 2.53]	0.58 ± 0.52	[0.07, 1.58]	1.24 ± 0.18	[1.01, 1.52]
59289	2.08 ± 1.55	[0.50, 5.03]	1.30 ± 1.25	[0.00, 3.64]	0.78 ± 0.62	[0.02, 1.99]	1.19 ± 0.23	[0.89, 1.59]
59431	1.51 ± 1.32	[0.35, 4.10]	0.68 ± 0.70	[0.06, 1.91]	0.83 ± 0.84	[0.14, 2.65]	1.28 ± 0.17	[1.07, 1.53]
59481	2.71 ± 1.87	[0.83, 6.25]	1.43 ± 1.13	[0.24, 3.52]	1.27 ± 1.01	[0.29, 3.21]	1.22 ± 0.11	[1.09, 1.41]
59493	2.07 ± 1.45	[0.51, 4.84]	1.10 ± 0.94	[0.11, 2.85]	0.97 ± 0.78	[0.16, 2.45]	1.14 ± 0.14	[0.95, 1.35]
G3101	3.38 ± 2.62	[0.95, 8.13]	2.26 ± 2.10	[0.28, 6.11]	1.11 ± 0.88	[0.25, 2.87]	1.17 ± 0.13	[1.00, 1.42]
K9400	1.11 ± 0.94	[0.26, 2.49]	0.56 ± 0.51	[0.06, 1.31]	0.55 ± 0.62	[0.06, 1.51]	1.23 ± 0.17	[0.96, 1.50]
W3467	1.39 ± 1.09	[0.29, 3.55]	0.77 ± 0.71	[0.08, 2.14]	0.62 ± 0.60	[0.08, 1.85]	1.41 ± 0.21	[1.12, 1.74]

Table S6 Trends of black carbon and its sources during the study period using the Theil−Sen method.

Code	eBC		eBC_{lf}		eBC_{sf}		Period
	μg m^{-3} yr^{-1}	% yr^{-1}	μg m^{-3} yr^{-1}	% yr^{-1}	μg m^{-3} yr^{-1}	% yr^{-1}	
52203	−0.18 [−0.35, −0.17] ***	−4.94 [−7.44, −4.82] ***	−0.08 [−0.13, −0.05] **	−4.55 [−6.49, −2.90] **	−0.12 [−0.21, −0.09] ***	−5.77 [−7.90, −4.92] ***	2008−2020
52418	−0.07 [−0.40, +0.22]	−1.91 [−6.24, +7.12]	−0.03 [−0.19, +0.11]	−1.79 [−5.59, +6.66]	−0.05 [−0.27, +0.19]	−2.11 [−8.67, +11.7]	2008−2017
53276	−0.08 [−0.17, −0.01] *	−8.04 [−12.0, −2.23] *	−0.05 [−0.09, −0.01] **	−8.80 [−11.7, −2.96] **	−0.03 [−0.06, +0.00] *	−7.07 [−10.7, −1.34] *	2008−2020
53787	+0.04 [−0.19, +0.27]	+3.13 [−7.46, +100]	+0.01 [−0.10, +0.17]	+1.92 [−6.74, −125]	+0.03 [−0.09, +0.11]	+6.34 [−7.21, +158]	2008−2019
54084	−0.13 [−0.21, −0.06] **	−6.56 [−8.64, −3.65] **	−0.05 [−0.08, −0.03] **	−6.55 [−8.98, −4.55] **	−0.08 [−0.12, −0.04] **	−6.95 [−8.18, −3.47] **	2008−2017
54102	−0.07 [−0.13, −0.03] *	−7.85 [−11.8, −5.81] *	−0.04 [−0.08, −0.01] *	−7.65 [−11.2, −2.42] *	−0.02 [−0.04, −0.02] *	−7.7 [−11.16, −6.23] *	2008−2017
54161	−0.08 [−0.37, +0.86]	−2.30 [−6.55, +86.9]	−0.06 [−0.20, +0.34]	−3.30 [−7.43, +38.7]	−0.01 [−0.19, +0.39]	−0.74 [−6.52, +80.4]	2008−2018
54339	−0.17 [−0.21, −0.11] ***	−5.49 [−6.44, −4.93] ***	−0.11 [−0.15, −0.08] ***	−6.05 [−7.03, −6.02] ***	−0.04 [−0.07, −0.03] **	−4.11 [−6.11, −2.95] **	2008−2020
54342	+0.16 [−0.16, +0.52]	+5.31 [−4.23, +42.0]	+0.06 [−0.15, +0.26]	+3.17 [−6.88, +24.5]	+0.09 [−0.02, +0.32]	+6.95 [−0.99, +89.9]	2008−2019
54346	+0.06 [−0.20, +0.33]	+1.75 [−5.39, +18.4]	−0.08 [−0.20, +0.17]	−3.79 [−9.14, +18.2]	+0.13 [+0.02, +0.22] *	+12.1 [+1.73, +34.0] *	2008−2019
54351	−0.11 [−0.25, +0.21]	−3.62 [−6.20, +9.40]	−0.11 [−0.19, +0.01]	−5.96 [−8.12, +0.60]	−0.01 [−0.09, +0.09]	−0.49 [−5.05, +8.67]	2008−2018
54421	−0.11 [−0.15, −0.03] *	−5.12 [−5.92, −1.37] *	−0.06 [−0.08, −0.04] ***	−5.12 [−5.92, −3.30] ***	−0.04 [−0.08, +0.03]	−4.39 [−6.05, +3.44]	2009−2020
54511	−0.03 [−0.50, +0.43]	−0.55 [−8.85, +17.7]	+0.00 [−0.40, +0.42]	+0.00 [−9.91, +131]	+0.00 [−0.12, +0.10]	−0.20 [−6.03, +7.91]	2008−2019
54662	−0.05 [−0.09, +0.22]	−2.94 [−4.66, +26.8]	+0.00 [−0.03, +0.21]	+0.01 [−3.95, −127]	−0.04 [−0.08, +0.01]	−4.27 [−5.70, +1.65]	2008−2020
54725	−0.56 [−1.25, +0.01]	−13.1 [−19.0, +0.69]	−0.32 [−0.73, +0.00]	−13.1 [−18.8, +0.19]	−0.22 [−0.64, +0.05]	−11.8 [−13.9, +17.9]	2008−2017
56294	−0.51 [−0.81, +0.04]	−6.40 [−8.28, +0.64]	−0.44 [−0.58, −0.13] *	−8.39 [−9.56, −3.00] *	−0.10 [−0.27, +0.24]	−3.76 [−6.79, +13.5]	2010−2020
56449	+0.00 [−0.01, +0.01]	−0.10 [−4.21, +9.37]	+0.00 [−0.01, +0.00]	−1.72 [−4.65, +7.99]	+0.00 [+0.00, +0.01]	+4.11 [−3.86, +26.6]	2009−2020
57083	−0.54 [−1.15, −0.07] *	−6.41 [−10.8, −1.12] *	−0.29 [−0.77, +0.03]	−6.69 [−11.4, +1.14]	−0.25 [−0.38, −0.07] *	−7.18 [−8.87, −2.73] *	2009−2019
57131	−0.50 [−0.86, +0.07]	−5.57 [−7.63, +1.13]	−0.38 [−0.70, +0.09]	−6.26 [−9.69, +1.99]	−0.18 [−0.29, −0.08] *	−5.73 [−8.30, −3.25] *	2008−2020
58448	−0.19 [−0.22, −0.15] **	−6.74 [−7.53, −5.81] **	−0.11 [−0.15, −0.07] **	−8.74 [−9.33, −6.51] **	−0.08 [−0.12, −0.01] *	−5.03 [−6.94, −0.52] *	2011−2020
58506	−0.10 [−0.16, −0.07] ***	−6.34 [−8.53, −4.52] ***	−0.06 [−0.10, −0.03] **	−6.48 [−9.07, −3.93] **	−0.04 [−0.07, −0.02] ***	−7.19 [−9.39, −4.36] ***	2008−2019
59431	−0.17 [−0.24, −0.14] ***	−5.50 [−6.77, −4.79] ***	−0.09 [−0.13, −0.07] ***	−5.54 [−6.66, −4.70] ***	−0.07 [−0.10, −0.06] ***	−5.22 [−6.18, −4.65] ***	2008−2020
59481	−0.53 [−0.74, −0.19] *	−7.80 [−9.74, −3.54] *	−0.40 [−0.52, −0.09] *	−9.25 [−9.67, −2.88] *	−0.13 [−0.30, −0.03] *	−5.40 [−8.49, −1.45] *	2008−2016
59493	−0.25 [−0.28, −0.23] ***	−8.71 [−9.67, −8.65] ***	−0.13 [−0.16, −0.08] **	−8.52 [−8.63, −5.88] **	−0.12 [−0.17, −0.08] ***	−9.32 [−11.6, −7.85] ***	2013−2020
W3467	−0.12 [−0.19, −0.06] ***	−5.56 [−7.95, −3.59] ***	−0.05 [−0.10, −0.02] **	−4.75 [−6.94, −1.64] **	−0.05 [−0.08, −0.02] ***	−5.83 [−7.53, −3.56] ***	2008−2020

*, **, and *** represent the trends that are significant at 0.05, 0.01, and 0.001 levels.

Table S7 Reported eBC mass concentrations, eBC_{sf} fraction, and AAE values from different observation networks and published papers.

Country	Site/code	Type	Lon	Lat	Alt (m)	Period	eBC	eBC_{sf}	AAE	Instrument	Matrix	Sources
India	Srinagar	U	74.83	34.13	1591	2017	4.3	0.22	1.31	AE31	PM_{10}	
India	Gulmarg	M	74.4	34.05	2703	2017	2.4	0.17	1.24	AE42-HS	PM_{10}	(Romshoo et al., 2023)
India	New Delhi	U	77.19	28.55	210	2017	12.3	0.26	1.35	AE33	PM_{10}	
Ireland	Carnsore Point		−6.35	52.17	0.217	2016−2017	0.32			AE33	PM_{10}	(Spohn et al., 2022)
India	Ranichauri		78.04	30.3	2200	2016	1.93			AE33	NP	(Pandey et al., 2020)
India	Chirbasa		79.08	30.98	3600	2016	0.395			AE33	NP	(Negi et al., 2019)
India	Ranichauri	B	78.08	30.25		2016−2018	1.74	0.34	1.42	AE33	$PM_{2.5}$	
India	Srinagar	V	78.08	34.08		2016−2018	11.7	0.23	1.30	AE33	$PM_{2.5}$	
India	Chandigarh	U	76.88	30.73		2016−2018	11.2	0.16	1.21	AE33	$PM_{2.5}$	
India	Varasi	U	83.01	25.3		2016−2018	8.68	0.27	1.34	AE33	$PM_{2.5}$	
India	Jodhpur	D	73.01	26.3		2016−2018	4.51	0.18	1.24	AE33	$PM_{2.5}$	
India	New Delhi	U	77.2	28.58		2016−2018	13.6	0.18	1.24	AE33	$PM_{2.5}$	
India	Ranchi	U	85.31	23.31		2016−2018	4.42	0.23	1.30	AE33	$PM_{2.5}$	
India	Kolkata	C	88.45	22.65		2016−2018	12.1	0.12	1.16	AE33	$PM_{2.5}$	(Kumar et al., 2020)
India	Guwahati	U	91.58	26.1		2016−2018	6.65	0.17	1.23	AE33	$PM_{2.5}$	
India	Bhuj	D	69.66	23.25		2016−2018	2.02	0.22	1.29	AE33	$PM_{2.5}$	
India	Pune	U	73.85	18.53		2016−2018	6.96	0.12	1.16	AE33	$PM_{2.5}$	
India	gpur	U	79.05	21.1		2016−2018	4.48	0.21	1.27	AE33	$PM_{2.5}$	
India	Visakhapatm	C	83.23	17.71		2016−2018	6.05	0.09	1.12	AE33	$PM_{2.5}$	
India	Thiruvananthapuram	C	76.95	8.48		2016−2018	4.65	0.19	1.25	AE33	$PM_{2.5}$	
India	Port Blair	BA	92.71	11.66		2016−2018	2.51	0.1	1.14	AE33	$PM_{2.5}$	
India	Vijayawada	SUB	80.62	16.44	30	2016	3.44	0.21	1.66	AE33		(Prasad et al., 2018)
India	Ahmednagar		74.74	19.09	649	2016	12.9	0.08	1.1	AE33	$PM_{2.5}$	(Kolhe et al., 2019)
India	Pashan		73.8	18.53	559	2016	6.07	0.13	1.17	AE33	$PM_{2.5}$	
Australia	Beresfield		151.67	−32.80	16	2015	1.27	0.15	1.20	AE33		(Duc et al., 2020)
Australia	Newcastle		151.76	−32.93	19	2015	0.97	0.17	1.23	AE33		
Czech	OK	RB	15.08	49.58	534	2015−2017	0.68	0.31	1.41	AE31	PM_{10}	(Mbengue et al., 2020)

Country	Site/code	Type	Lon	Lat	Alt (m)	Period	eBC	eBC_{sf}	AAE	Instrument	Matrix	Sources
Polar	Syowa	P	39.35	−69.00	29	2015−2017	0.0034			AE31		(Hara et al., 2019)
Spain	Barcelo	U	2.12	41.39	80	2015−2017	1.49	0.08	1.17	AE33	PM_{10}	(Savadkoohi et al., 2023)
Switzerland	Bern-Bollwerk	TRA	7.44	46.95	536	2015−2017	1.09	0.28	1.20	AE33	$PM_{2.5}$	
Romania	Bucharest	SUB	26.03	44.35	70	2016, 2017	2.07	0.34	1.44	AE33	PM_{10}	
Spain	Grada	U	−3.58	37.18	680	2015, 2016	2.62	0.19	1.28	AE33	Aerosol	
Sweden	Hornsgatan	U	18.05	59.32	669	2015−2017	1.09	0.11	1.15	AE33	PM_{10}	
Spain	Madrid	SUB	−3.73	40.46	162	2015−2017	1.70	0.13	1.19	AE33	PM_1/$PM_{2.5}$	
France	Paris	U	2.16	48.71	25	2015−2017	0.76	0.23	1.38	AE33	$PM_{2.5}$	
Sweden	Torkel	U	18.06	59.32	48	2015−2017	0.33	0.23	1.32	AE33	PM_1	
Switzerland	Zurich	UB	8.53	47.38	409	2015−2017	1.01	0.23	1.31	AE33	$PM_{2.5}$	
UK	UKA00451	RB	−3.24	55.79	260	2015−2017	0.15	0.29	1.29	AE22	$PM_{2.5}$	UK AIR
UK	UKA00503	UB	−6.25	54.86	59	2015−2017	0.91	0.40	1.48	AE22	$PM_{2.5}$	
UK	UKA00212	UB	−5.93	54.60	10	2015−2017	1.09	0.19	1.26	AE22	$PM_{2.5}$	
UK	UKA00655	UB	−1.83	52.51	134	2015−2017	1.14	0.13	1.19	AE22	$PM_{2.5}$	
UK	UKA00626	TRA	−1.83	52.51	93	2015−2017	2.11	0.08	1.12	AE22	$PM_{2.5}$	
UK	UKA00217	UB	−3.18	51.48	12	2015−2017	0.88	0.19	1.25	AE22	$PM_{2.5}$	
UK	UKA00614	RB	−1.44	51.15	78	2015−2017	0.39	0.37	1.44	AE22	$PM_{2.5}$	
UK	UKA00481	RB	0.58	51.31	182	2015−2017	0.47	0.26	1.33	AE22	$PM_{2.5}$	
UK	UKA00602	TRA	−4.24	55.86	35	2015−2017	1.51	0.10	1.14	AE22	$PM_{2.5}$	
UK	UKA00576	UB	−4.24	55.87	40	2015−2017	0.84	0.10	1.13	AE22	$PM_{2.5}$	
UK	UKA00570	UB	−6.01	54.54	35	2015−2017	0.71	0.31	1.40	AE22	$PM_{2.5}$	
UK	UKA00315	TRA	−0.15	51.52	35	2015−2017	4.67	0.06	1.09	AE22	$PM_{2.5}$	
UK	UKA00253	UB	−0.21	51.52	5	2015−2017	1.01	0.19	1.25	AE22	$PM_{2.5}$	
UK	UKA00393	SUBB	−7.45	54.82	28	2015−2017	1.22	0.48	1.57	AE22	$PM_{2.5}$	
USA	2916	SUB	−71.36	41.84	15	2015−2017	0.41			AE16	$PM_{2.5}$	US EPA
USA	48101	SUB	−83.21	42.23	181	2015−2017	0.57			AE21	$PM_{2.5}$	

Country	Site/code	Type	Lon	Lat	Alt (m)	Period	eBC	eBC_{sf}	AAE	Instrument	Matrix	Sources
USA	7002	U	−74.13	40.67	3	2015–2017	1.20			AE33	$PM_{2.5}$	
USA	94710	U	−122.30	37.86	2.7	2015–2017	1.14			AE33	$PM_{2.5}$	
USA	63107	U	−90.20	38.66	150	2015–2017	0.82	0.32	1.41	AE33	$PM_{2.5}$	
USA	64133	SUB	−94.45	39.05	293	2015–2017	0.86	0.23	1.32	AE33	$PM_{2.5}$	
USA	84010	SUB	−111.88	40.90	1309	2015–2017	0.64			AE21	$PM_{2.5}$	
USA	8103	U	−75.13	39.93	4	2015–2017	0.75			AE33	$PM_{2.5}$	
USA	2905	U	−71.41	41.81	9	2015–2017	0.37			AE16	$PM_{2.5}$	
USA	45225	U	−84.54	39.15	162	2015–2017	2.10			AE33	$PM_{2.5}$	
USA	6513	U	−72.90	41.30	3.6	2015–2017	0.67	0.23	1.32	AE33	$PM_{2.5}$	
USA	2119	U	−71.08	42.33	6	2015–2017	0.72			AE33	$PM_{2.5}$	
USA	48223	U	−83.27	42.39	0.5	2015–2017	0.61	0.46	1.56	AE33	$PM_{2.5}$	
USA	7202	SUB	−74.21	40.64	5	2015–2017	1.58			AE33	$PM_{2.5}$	
USA	48223	SUB	−83.27	42.39	0.5	2015–2017	1.06	0.26	1.35	AE33	$PM_{2.5}$	
USA	46517	RU	−85.97	41.66	197	2015–2017	0.44	0.57	1.67	AE22ER	$PM_{2.5}$	
USA	47710	SUB	−87.58	38.01	116	2015–2017	0.48	0.64	1.73	AE22ER	$PM_{2.5}$	
USA	94933	SUB	−122.69	38.02	75	2015–2017	0.82			AE33	$PM_{2.5}$	US EPA
USA	63110	U	−90.28	38.63	310	2015–2017	0.93	0.25	1.34	AE33	$PM_{2.5}$	
USA	7024	U	−73.97	40.85	87	2015–2017	0.82			AE33	$PM_{2.5}$	
USA	46403	SUB	−87.30	41.61	122	2015–2017	0.69	0.22	1.31	AE21ER	$PM_{2.5}$	
USA	1301	U	−72.60	42.61	267	2015–2017	0.46			AE33	$PM_{2.5}$	
USA	6120	U	−72.68	41.77	8	2015–2017	0.90	0.29	1.39	AE33	$PM_{2.5}$	
USA	80204	SUB	−105.02	39.73	1583	2015–2017	1.84	0.09	1.14	AE33	$PM_{2.5}$	
USA	46218	U	−86.11	39.81	230	2015–2017	0.62	0.37	1.48	AE21ER	$PM_{2.5}$	
USA	46201	U	−86.13	39.79	195	2015–2017	1.20	0.25	1.34	AE33	$PM_{2.5}$	
USA	10455	U	−73.90	40.82	17	2015–2017	0.88			AE21ER	$PM_{2.5}$	
USA	94607	U	−122.26	37.79	3.9	2015–2017	1.27			AE33	$PM_{2.5}$	
USA	1104	U	−72.59	42.11	31	2015–2017	0.87			AE33	$PM_{2.5}$	
USA	94551	U	−121.78	37.69	137	2015–2017	0.65			AE33	$PM_{2.5}$	
USA	48152	SUB	−83.43	42.42	0.1	2015–2017	0.61	0.43	1.54	AE33	$PM_{2.5}$	
USA	6108	U	−72.63	41.78	15	2015–2017	0.48	0.34	1.44	AE33	$PM_{2.5}$	
USA	20001	SUB	−77.01	38.92	50	2015–2017	0.63		1.47	AE21	$PM_{2.5}$	

Country	Site/code	Type	Lon	Lat	Alt (m)	Period	eBC	eBC_{sf}	AAE	Instrument	Matrix	Sources
USA	27616	U	−78.57	35.86	100	2015–2017	0.44	0.09	1.14	AE21ER	$PM_{2.5}$	
USA	19801	RU	−75.56	39.74	0	2015–2017	0.65			AE33	$PM_{2.5}$	
USA	6759	SUB	−73.30	41.82	505	2015–2017	0.20	0.36	1.46	AE33	$PM_{2.5}$	
USA	33607	U	−82.47	27.96	6	2015–2017	0.92			AE33	$PM_{2.5}$	
USA	2908	U	−71.42	41.83	23	2015–2017	1.64			Multiple	$PM_{2.5}$	
USA	55404	U	−93.25	44.97	259	2015–2017	0.87	0.23	1.32	AE33	$PM_{2.5}$	
USA	2109	SUB	−71.05	42.36	7	2015–2017	0.90			Multiple	$PM_{2.5}$	
USA	30034	U	−84.27	33.70	238	2015–2017	1.86			MAAP	$PM_{2.5}$	
USA	30313	U	−84.39	33.78	286	2015–2017	2.22			MAAP	$PM_{2.5}$	
USA	94607	SUB	−122.28	37.81	0	2015–2017	0.70			AE33	$PM_{2.5}$	
USA	15221	SUB	−79.86	40.44	355	2015–2017	0.99	0.17	1.24	AE33	$PM_{2.5}$	
USA	48120	U	−83.15	42.31	0	2015–2017	0.78			AE21	$PM_{2.5}$	
USA	14610	RU	−77.55	43.15	137	2015–2017	0.35			AE21ER	$PM_{2.5}$	US EPA
USA	28138	U	−80.40	35.55	240	2015–2017	0.44	0.26	1.36	AE22ER	$PM_{2.5}$	
USA	95814	SUB	−121.50	38.59	12.8	2015–2017	1.20			AE33	$PM_{2.5}$	
USA	95821	U	−121.37	38.61	8	2015–2017	0.63			AE33	$PM_{2.5}$	
USA	95122	SUB	−121.85	37.34	30.9	2015–2017	1.00			AE33	$PM_{2.5}$	
USA	33702	U	−82.67	27.83	15	2015–2017	0.64			AE33	$PM_{2.5}$	
USA	98104	U	−122.32	47.60	15	2015–2017	1.49	0.19	1.27	AE33	$PM_{2.5}$	
USA	98144	U	−122.33	47.60	26	2015–2017	1.05	0.31	1.41	AE33	$PM_{2.5}$	
USA	98144	SUB	−122.31	47.60	58	2015–2017	0.80	0.29	1.38	AE33	$PM_{2.5}$	
USA	33782	SUB	−82.71	27.85	4.41	2015–2017	0.40			AE33	$PM_{2.5}$	
USA	30034	SUB	−84.29	33.69	308	2015–2017	1.19			AE21	$PM_{2.5}$	
USA	97224	SUB	−122.75	45.39	53	2015–2017	1.13	0.34	1.44	Multiple	$PM_{2.5}$	
USA	2125	U	−71.06	42.33	15	2015–2017	1.21			AE33	$PM_{2.5}$	
USA	6810	SUB	−73.44	41.40	116	2015–2017	0.66	0.36	1.47	AE33	$PM_{2.5}$	
Australia	AU0002G	C	144.69	−40.68	94	2015–2017	0.04			MAAP	PM_{1}	
Bulgaria	BG0001R	NP	23.58	42.17	2971	2015–2017	0.18			CLAP-10	Aerosol	
Bolivia	BO0001R	NP	−68.10	−16.20	5320	2015–2017	0.07	0.16	1.02	AE31	PM10	EBAS
Cada	CA0011R	RU	−79.78	44.23	255	2015–2017	0.26			CLAP-10	PM_{1}	
Cada	CA0420G	P	−62.34	82.50	210	2015–2017	0.01	0.09	0.93	AE31	Aerosol	

Country	Site/code	Type	Lon	Lat	Alt (m)	Period	eBC	eBC_{sf}	AAE	Instrument	Matrix	Sources
Switzerland	CH0001G	M	7.99	46.55	3578	2015–2017	0.02	0.12	1.09	AE33	Aerosol	
Switzerland	CH0002R	RU	6.94	46.81	489	2015–2017	0.68	0.24	1.33	AE33	$PM_{2.5}$	
Switzerland	CH0005R	NP	8.46	47.07	1031	2015–2017	0.25	0.22	1.36	AE33	$PM_{2.5}$	
Chile	CL0001R	M	−70.80	−30.17	2220	2015–2017	0.04	0.18	1.14	AE31	Aerosol	
Cyprus	CY0002R	RU	33.06	35.04	520	2015–2017	0.11	0.06	0.95	AE31	Aerosol	
Czech	CZ0003R	RU	15.08	49.57	535	2015–2017	0.16	0.18	1.15	AE31	PM_{10}	
Germany	DE0002R	NP	10.76	52.80	74	2015–2017	0.54			MAAP	PM_{10}	
Germany	DE0003R	NP	7.91	47.91	1205	2015–2017	0.42			MAAP	PM_{10}	
Germany	DE0003R	NP	7.91	47.91	1205	2015–2017	0.42			MAAP	PM_{1}	
Germany	DE0007R	NP	13.03	53.17	62	2015–2017	0.43			MAAP	PM_{10}	
Germany	DE0043G	M	11.01	47.80	975	2015–2017	0.35			MAAP	PM_{10}	
Germany	DE0044R	RU	12.93	51.53	86	2015–2017	0.65			MAAP	PM_{10}	
Germany	DE0054R	M	10.98	47.42	2671	2015–2017	0.10			MAAP	PM_{10}	
Germany	DE0055B	NP	12.43	51.35	113	2015–2017	0.93			MAAP	PM_{10}	
Germany	DE0060G	P	−8.27	−70.67	42	2015–2017	0.00			MAAP	Aerosol	
Germany	DE0066K	NP	12.41	51.35	120	2015–2017	1.58			MAAP	PM_{1}	EBAS
Germany	DE0066K	NP	12.41	51.35	120	2015–2017	1.58			MAAP	PM_{10}	
Germany	DE0067K	NP	12.38	51.34	111	2015–2017	2.15			MAAP	PM_{10}	
Germany	DE0068B	NP	12.30	51.32	122	2015–2017	0.46			MAAP	PM_{10}	
Denmark	DK0025G	P	−38.48	72.58	3238	2015–2017	0.01			CLAP-10	$PM_{2.5}$	
Spain	ES0018G	M	−16.50	28.31	2373	2015–2017	0.16			MAAP	PM_{10}	
Spain	ES0020U	NP	−3.61	37.16	680	2015–2017	2.35			MAAP	PM_{10}	
Spain	ES0022R	M	0.73	42.05	1571	2015–2017	0.20			MAAP	PM_{10}	
Spain	ES0100R	RU	−6.73	37.10	41	2015–2017	0.42			CLAP-10	PM_{1}	
Spain	ES1778R	NP	2.35	41.77	700	2015–2017	0.36			MAAP	PM_{10}	
Spain	ES1778R	NP	2.35	41.77	700	2015–2017	0.36			MAAP	Aerosol	
Finland	FI0050R	RU	24.28	61.85	181	2015–2017	0.05	0.08	0.93	AE31	PM_{10}	
Finland	FI0096G	RU	24.12	67.97	565	2015–2017	0.02	0.11	0.92	AE31	Aerosol	
France	FR0019R	NP	0.14	42.94	2877	2015–2017	0.01			AE16	PM_{10}	
France	FR0019R	NP	0.14	42.94	2877	2015–2017	0.01			AE16	Aerosol	
France	FR0022R	RU	5.51	48.56	392	2015–2017	0.09	0.13	1.16	AE31	Aerosol	

Country	Site/code	Type	Lon	Lat	Alt (m)	Period	eBC	eBC_{sf}	AAE	Instrument	Matrix	Sources
France	FR0026R	M	55.38	−21.08	2160	2015−2017	0.07	0.15	1.15	AE42	PM_{10}	
France	FR0030R	M	2.96	45.77	1465	2015−2017	0.19			MAAP	Aerosol	
Greece	GR0100B	U	23.82	37.99	270	2015−2017	0.36	0.69	1.16	AE33	PM_{10}	
Greece	GR0101R	M	22.20	37.98	2340	2015−2017	0.03			AE31	PM_{10}	
Hungary	HU0002R	RU	19.58	46.97	125	2015−2017	1.20			CLAP-10	PM_{10}	
Ireland	ID1013R	M	100.32	−0.20	845	2015−2017	0.22	0.16	1.22	AE31	Aerosol	
Italy	IT0009R	M	10.70	44.19	2165	2015−2017	0.22			MAAP	Aerosol	
R. Koera	KR0100R	C	126.33	36.54	46	2015−2017	0.28	0.12	1.10	AE31	PM_{10}	
Netherlands	NL0011R	NP	4.93	51.97	1	2015−2017	0.43			MAAP	PM_{10}	
Norway	NO0002R	RU	8.25	58.39	219	2015−2017	0.63			PSAP-1W	PM_{10}	
Norway	NO0002R	RU	8.25	58.39	219	2015−2017	0.63			PSAP-3W	PM_{10}	
Norway	NO0042G	P	11.89	78.91	474	2015−2017	0.01	0.04	0.36	AE31	PM_{10}	EBAS
Norway	NO0059G	P	2.54	−72.01	1553	2015−2017	0.01			PSAP-3W	PM_{10}	
Puerto Rico	PR0100C	NP	−65.62	18.38	65	2015−2017	0.09			CLAP−10	PM_{1}	
Russia	RU0100R	C	128.92	71.59	8	2015−2017	0.10			MAAP	PM_{10}	
Chi	TW0100R	NP	120.87	23.47	2862	2015−2017	0.51			PSAP-3W	PM_{1}	
USA	US0035R	NP	−88.37	40.05	213	2015−2017	0.29			CLAP-10	PM_{1}	
USA	US3446C	NP	−81.70	36.20	1100	2015−2017	0.26			PSAP-3W	PM_{1}	
USA	US3446C	NP	−81.70	36.20	1100	2015−2017	0.26			CLAP-10	PM_{1}	
USA	US6002C	RU	−97.48	36.61	318	2015−2017	0.26			PSAP-3W	PM_{1}	
USA	US6005G	C	−124.15	41.05	107	2015−2017	0.07			CLAP-10	PM_{1}	
USA	US9050R	M	−106.74	40.45	3220	2015−2017	0.08			CLAP-10	PM_{1}	
Viet m	VN0001R	M	103.52	21.57	1466	2015−2017	0.34	0.46	1.46	AE31	Aerosol	

B: Background; BA: Bay; C: Coastal; D: Desert; M: Mountain; NP: Not provided; P: Polar; RB: Rural background; RU: Rural; SUB: Suburban; SUBB: Suburban background; TRA: Traffic; U: Urban; UB: Urban background; V: Valley

Table S8 The detailed information about the station with the continuous measurements of BC from 2008 to 2020 in this study and previous studies or observation networks.

Site me/code	Country	Type [a]	Lon	Lat	Period	Instrument	Slope (% yr^{-1})	Sources
Zabrze	Poland	UB	18.20	50.10	2010−2020	MAAP	−1.46	(Chilinski et al., 2016)
RB2	Finland	RB	24.28	61.85	2008−2018	MAAP&AE31	−6.54	(Luoma et al., 2021)
St. Louis	USA	U	−90.20	38.66	2008−2015	AE21 &AE33	+4.40	US EPA
Providence-Warwick, RI-MA	USA	U	−71.41	41.81	2008−2020	AE16	−3.57	
Boston	USA	U	−71.08	42.33	2008−2020	AE21ER & AE33	−2.22	
Elkhart	USA	RU	−85.97	41.66	2012−2020	AE22	−1.33	
Evansville	USA	SUB	−87.58	38.01	2009−2020	AE22	−1.91	
Lagunitas	USA	SUB	−122.69	38.02	2013−2020	AE22 & AE33	−4.46	
East Providence	USA	SUB	−71.36	41.84	2008−2020	AE16 &AE33	−2.47	
Gary	USA	SUB	−87.30	41.61	2008−2020	AE21	−4.04	
Indiapolis	USA	U	−86.11	39.81	2008−2020	AE21	−3.06	
New York	USA	U	−73.90	40.82	2008−2018	AE21	−4.51	
Springfield	USA	U	−72.59	42.11	2008−2018	AE22 & AE33	−1.08	
Livermore	USA	U	−121.78	37.69	2012−2020	AE16 &AE33	−2.70	
Washington	USA	SUB	−77.01	38.92	2008−2020	AE22 & AE33	−3.41	
Wilmington	USA	RU	−75.56	39.74	2008−2019	AE22 & AE33	−3.89	
Oakland	USA	SUB	−122.28	37.81	2009−2020	AE22 & AE33	−3.07	
Rochester	USA	RU	−77.55	43.15	2008−2018	AE21	−4.72	
Arden−Arcade	USA	U	−121.37	38.61	2008−2020	Multiple	−2.34	
South DeKalb	USA	SUB	−84.29	33.69	2008−2016	AE21ER	−2.63	
DDN	Germany	R	13.74	51.07	2009−2018	MAAP	−11.30	(Sun et al., 2020)
LEI	Germany	R	12.41	51.35	2009−2018	MAAP	−5.00	
LMI	Germany	R	12.38	51.34	2010−2018	MAAP	−5.50	
LTR	Germany	UB	12.43	51.35	2009−2018	MAAP	−4.10	
ANA	Germany	UB	13.00	50.57	2012−2018	MAAP	−6.90	
AUG	Germany	UB	10.91	48.36	2009−2018	Aethalometer	−2.30	
DDW	Germany	UB	13.73	51.04	2012−2018	MAAP	−8.10	
BOS	Germany	UB	7.94	53.00	2009−2014	MAAP	−4.90	
MEL	Germany	RB	12.93	51.53	2009−2018	MAAP	−4.40	
WAL	Germany	RB	10.76	52.80	2009−2018	MAAP	−3.20	
NEU	Germany	RB	13.03	53.14	2010−2018	MAAP	−7.80	
HPB	Germany	M	11.01	47.80	2009−2018	MAAP	−2.80	

Site me/code	Country	Type [a]	Lon	Lat	Period	Instrument	Slope (% yr^{-1})	Sources
SCH	Germany	M	7.91	47.91	2009−2018	MAAP	−1.70	(Sun et al., 2020)
ZSF	Germany	M	10.98	47.42	2009−2018	MAAP	−4.00	
BCN	Spain	UB	2.12	41.39	2012−2020	AE33	−5.37	(Savadkoohi et al., 2023)
GRA	Spain	UB	−3.58	37.18	2012−2020	MAAP&AE33	−2.41	
LND	UK	UB	−0.21	51.52	2012−2020	AE22 & AE33	−8.32	
LEJ	Germany	UB	12.43	51.35	2012−2020	MAAP	−3.60	
NLD	Netherlands	UB	4.49	51.89	2012−2020	MAAP	−4.79	
ZUR	Switzerland	UB	8.53	47.38	2012−2020	AE33	−10.0	
LND	UK	TRA	−0.15	51.52	2012−2020	AE22 & AE33	−10.5	
LEJ	Germany	TRA	12.41	51.35	2012−2020	MAAP	−3.30	
NLD	Netherlands	TRA	4.48	51.89	2012−2020	MAAP	−6.06	
NLD	Netherlands	TRA	4.48	51.91	2012−2020	MAAP	−5.42	
PAR	France	SUB	2.16	48.71	2012−2020	AE33	−5.92	
IPR	Italy	RB	8.63	45.80	2012−2020	MAAP	−3.28	
SMR	Finland	RB	24.30	61.85	2012−2020	AE31 & AE33 & MAAP	−6.36	
Bern-Bollwerk	Switzerland	TRA	7.44	46.95	2013−2018	AE31&AE33	−11.3	(Grange et al., 2020)
Zirich-K aserne	Switzerland	TRA	8.53	47.38	2009−2018	AE31&AE33	−6.36	
Payerne	Switzerland	RU	6.94	46.81	2008−2018	AE31&AE33	+3.00	
Magadino-Cadezzo	Switzerland	RU	8.93	46.16	2008−2018	AE31&AE33	−1.58	
San Vittore	Switzerland	RU	9.11	46.24	2013−2018	AE33	−2.64	
Rigi-Seebodelp	Switzerland	M	8.46	47.07	2013−2018	AE33	−10.8	
Auchencorth Moss	UK	RB	−3.24	55.79	2012−2020	AE22	−6.08	UK AIR
Ballymena Ballykeel	UK	UB	−6.25	54.86	2013−2020	AE22	−7.19	
Belfast Centre	UK	UB	−5.93	54.60	2009−2020	AE22	−5.38	
Birmingham Tyburn	UK	UB	−1.83	52.51	2009−2017	AE22	−3.73	
Detling	UK	RB	0.58	51.31	2012−2020	AE22	−3.95	
Glasgow Townhead	UK	UB	−4.24	55.87	2013−2020	AE22	−5.03	
Kilmakee Leisure Centre	UK	UB	−6.01	54.54	2012−2020	AE22	−5.51	
London Marylebone Road	UK	TR	−0.15	51.52	2009−2020	AE22	−7.83	
London N. Kensington	UK	TR	−0.21	51.52	2009−2020	AE22	−5.68	
Strabane 2	UK	SUBB	−7.45	54.82	2009−2020	AE22	−2.10	

B: baseline; M: Mountain; R: Roadside; RB: Rural background; Ru: Rural; SUB: SUB; SUBB: SUB background; TR: Traffic; U: U; UB: U background

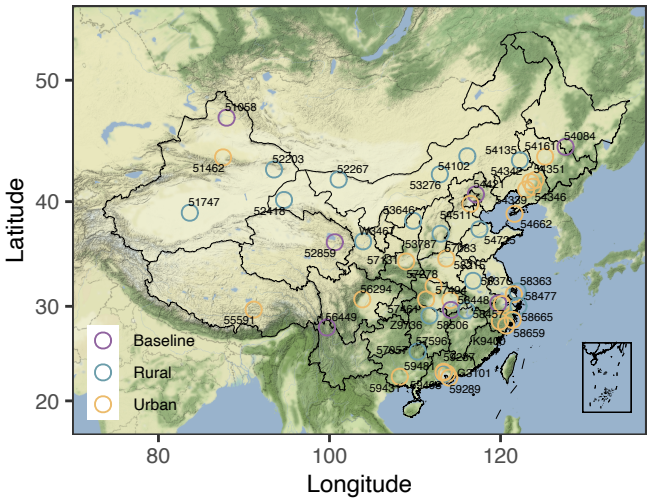

Figure S1 Spatial distribution in BC observational stations in this study.

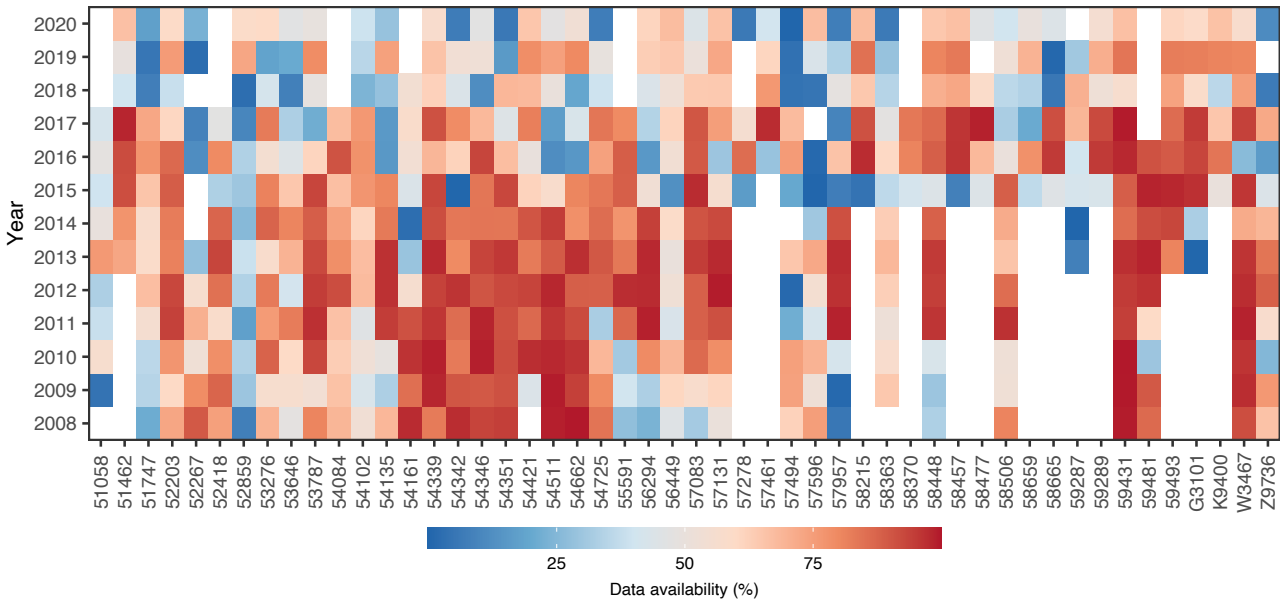

Figure S2 Data availability of black carbon in each station during the observational period from 2008 to 2020.

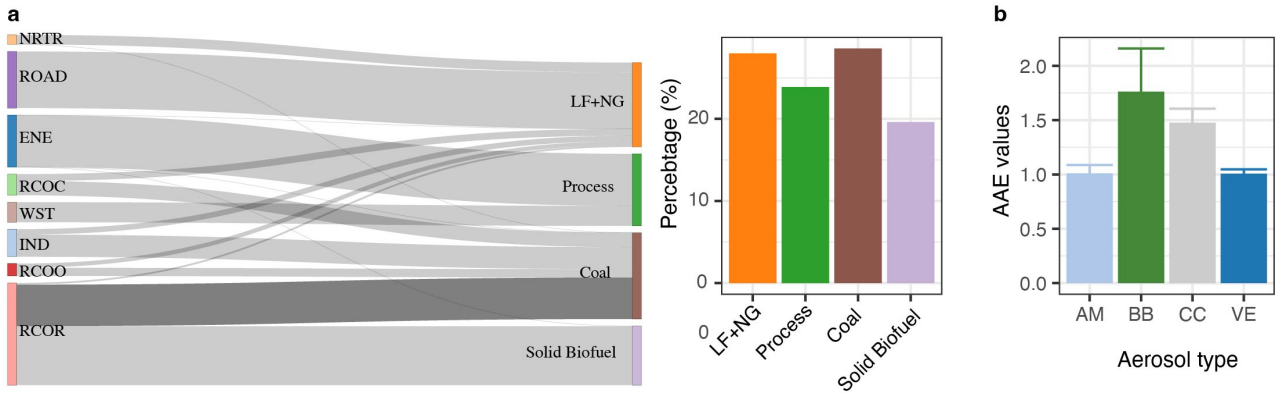

Figure S3 Black carbon from different sectors and fuel types and their percentage to total BC emissions (a) and AAE from different types of aerosols including ambient air (AM), biomass burning (BB), coal combustion (CC), and vehicle emissions (VE) from our unpublished data. The data and more details about the sectors and fuel types can be found in McDuffie et al. (2020).

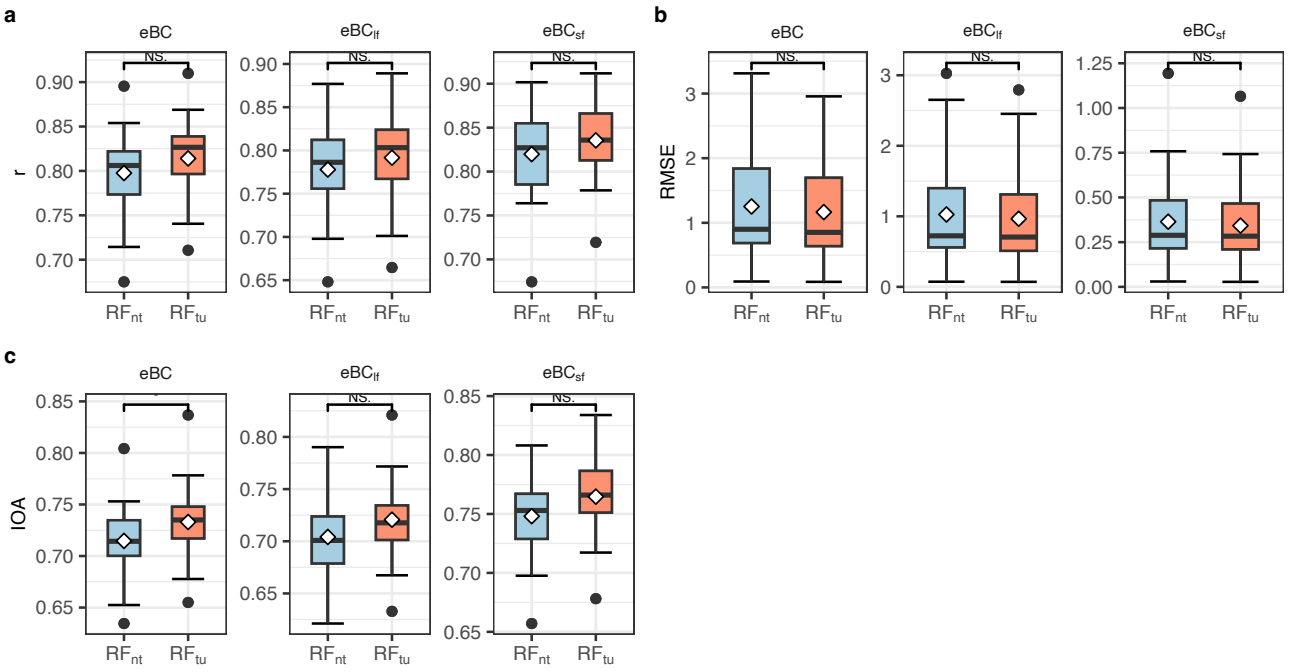

Figure S4 Comparison of model performance evaluation statistics for eBC, eBC$_{lf}$, and eBC$_{sf}$ by the random forest with parameters not tunned (RF$_{nt}$) and tuned (RF$_{tu}$).

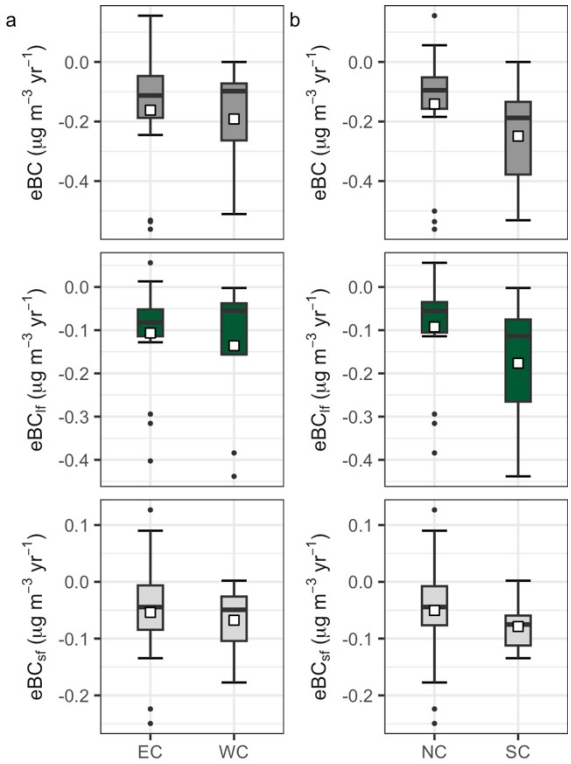

Figure S5 Comparisons of trends of black carbon (eBC) concentration and its sources including liquid fuel (eBC_{lf}) and solid fuel (eBC_{sf}) combustion between eastern China (EC), western China (WC), northern China (NC) and southern China (SC).

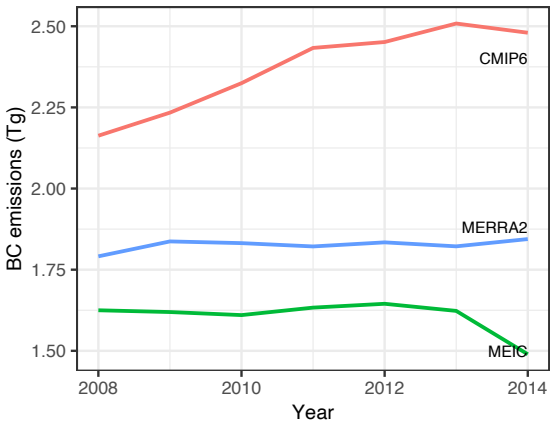

Figure S6 Black carbon emissions in China from different emission inventories from 2008 to 2014.

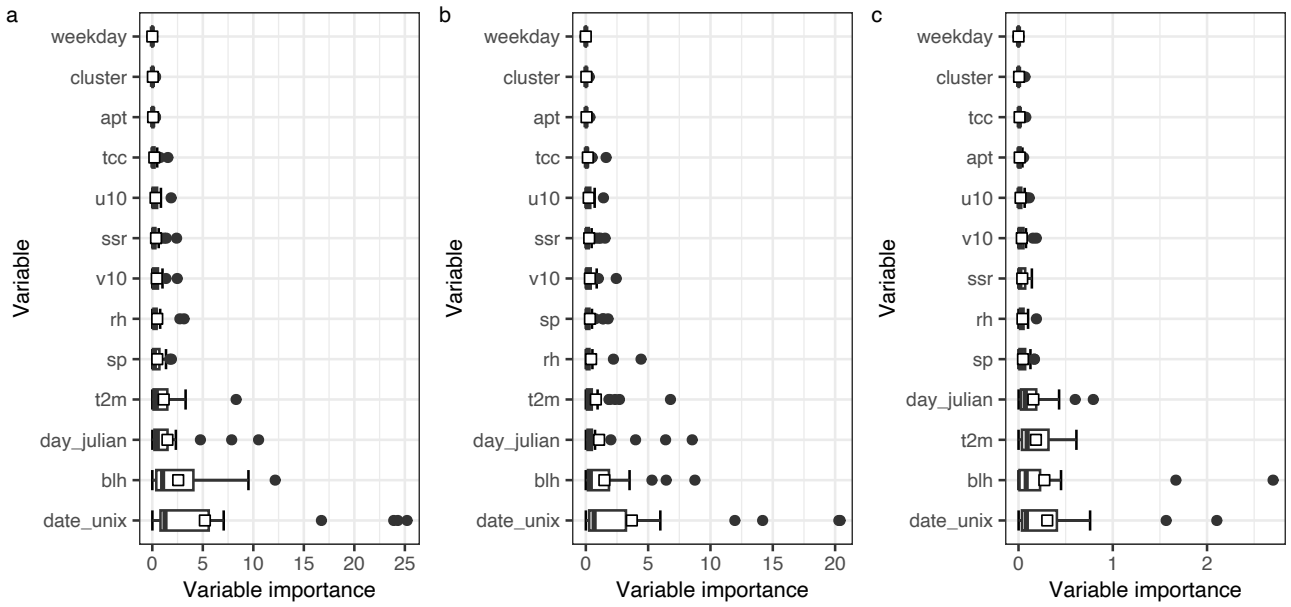

Figure S7 Variable importance for the 25 BC monitoring sites' random forest models for eBC (a), eBC_{lf} (b), and eBC_{sf} (c)

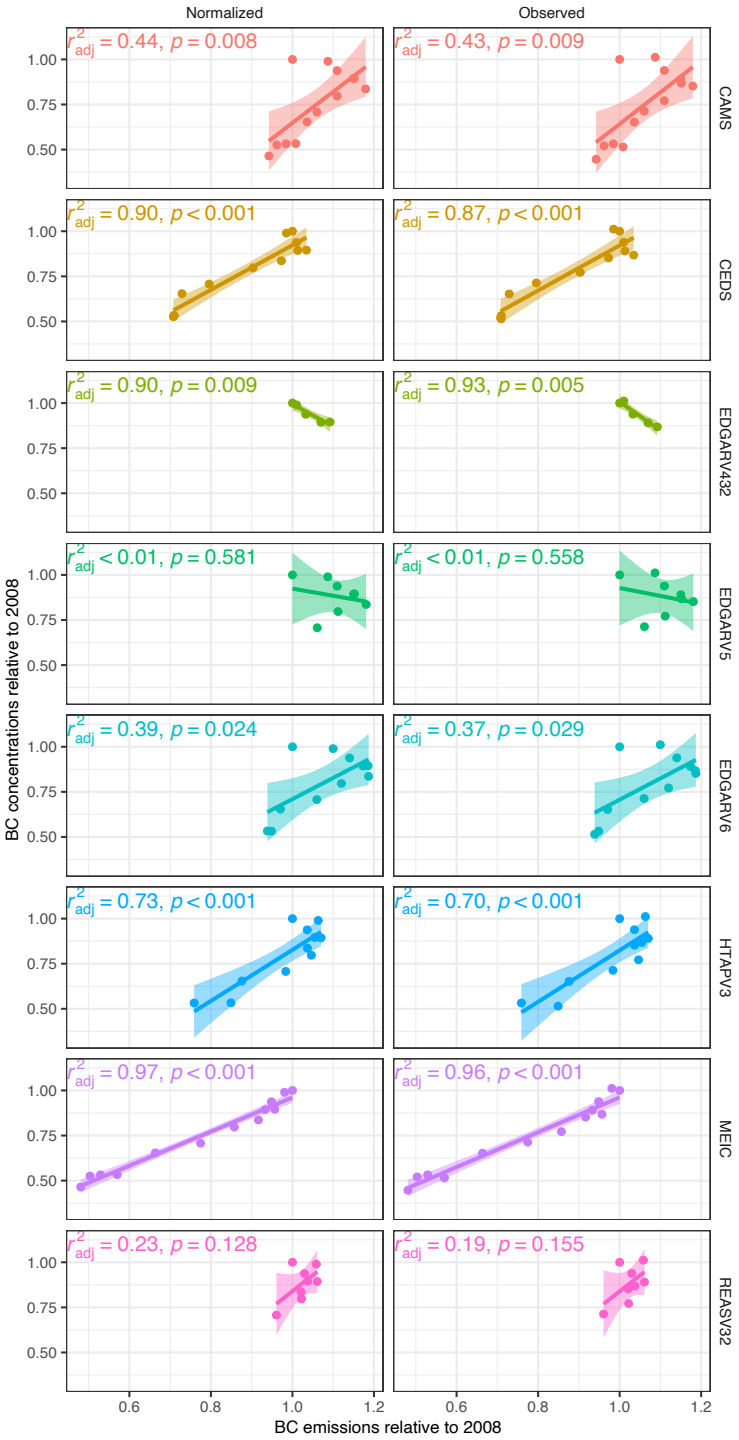

Figure S8 Scatterplot between observed and weather normalized BC concentrations and their emissions from different inventories.

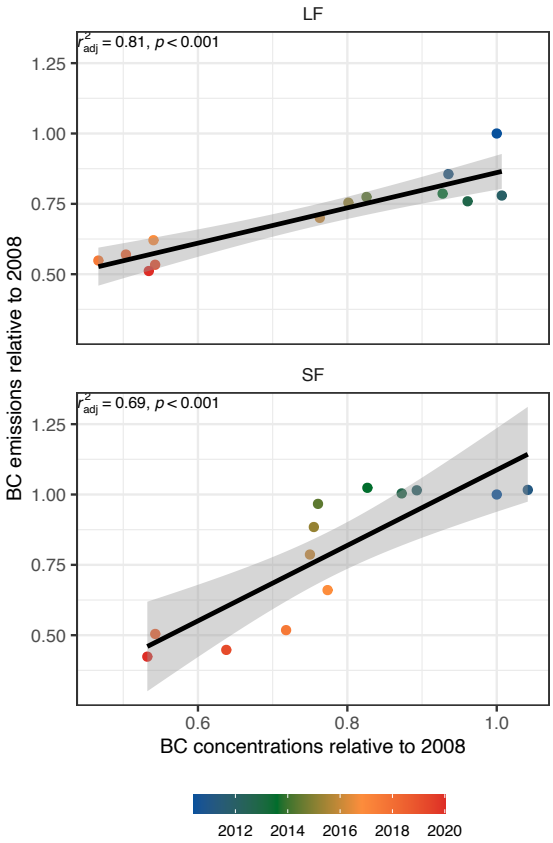

Figure S9 Scatterplot between weather normalized BC source concentrations (including liquid fuel (LF) and solid fuel (SF)) and their emissions derived from MEIC.

References

Chilinski, M. T., Markowicz, K. M., and Markowicz, J.: Observation of vertical variability of black carbon concentration in lower troposphere on campaigns in Poland, Atmos. Environ., 137, 155–170, https://doi.org/10.1016/j.atmosenv.2016.04.020, 2016.

Duc, H. N., Shingles, K., White, S., Salter, D., Chang, L. T.-C., Gunashanhar, G., Riley, M., Trieu, T., Dutt, U., Azzi, M., Beyer, K., Hynes, R., and Kirkwood, J.: Spatial-Temporal Pattern of Black Carbon (BC) Emission from Biomass Burning and Anthropogenic Sources in New South Wales and the Greater Metropolitan Region of Sydney, Australia, Atmosphere, 11, 570, https://doi.org/10.3390/atmos11060570, 2020.

Grange, S. K., Lotscher, H., Fischer, A., Emmenegger, L., and Hueglin, C.: Evaluation of equivalent black carbon source apportionment using observations from Switzerland between 2008 and 2018, Atmos. Meas. Tech., 13, 1867–1885, https://doi.org/10.5194/amt-13-1867-2020, 2020.

Hara, K., Sudo, K., Ohnishi, T., Osada, K., Yabuki, M., Shiobara, M., and Yamanouchi, T.: Seasonal features and origins of carbonaceous aerosols at Syowa Station, coastal Antarctica, Atmos. Chem. Phys., 19, 7817–7837, https://doi.org/10.5194/acp-19-7817-2019, 2019.

Kolhe, A. R., Ralegankar, S. D., Safai, P. D., and Aher, G. R.: Absorption properties of black carbon aerosols over environmentally distinct locations in south-western India: Temporal, spectral characterization and source apportionment, J. Atmos. Sol. Terr. Phys., 189, 1–17, https://doi.org/10.1016/j.jastp.2019.03.010, 2019.

Kumar, R. R., Soni, V. K., and Jain, M. K.: Evaluation of spatial and temporal heterogeneity of black carbon aerosol mass concentration over India using three year measurements from IMD BC observation network, Sci. Total Environ., 723, 138060, https://doi.org/10.1016/j.scitotenv.2020.138060, 2020.

Luoma, K., Niemi, J. V., Aurela, M., Fung, P. L., Helin, A., Hussein, T., Kangas, L., Kousa, A., Rönkkö, T., Timonen, H., Virkkula, A., and Petäjä, T.: Spatiotemporal variation and trends in equivalent black carbon in the Helsinki metropolitan area in Finland, Atmos. Chem. Phys., 21, 1173–1189, https://doi.org/10.5194/acp-21-1173-2021, 2021.

McDuffie, E. E., Smith, S. J., O'Rourke, P., Tibrewal, K., Venkataraman, C., Marais, E. A., Zheng, B., Crippa, M., Brauer, M., and Martin, R. V.: A global anthropogenic emission inventory of atmospheric pollutants from sector- and fuel-specific sources (1970–2017): an application of the Community Emissions Data System (CEDS), Earth Syst. Sci. Data, 12, 3413–3442, https://doi.org/10.5194/essd-12-3413-2020, 2020.

Mbengue, S., Serfozo, N., Schwarz, J., Ziková, N., Šmejkalová, A. H., and Holoubek, I.: Characterization of equivalent black carbon at a regional background site in Central Europe: Variability and source apportionment, Environ. Pollut., 260, 113771, https://doi.org/10.1016/j.envpol.2019.113771, 2020.

Negi, P. S., Pandey, C. P., and Singh, N.: Black carbon aerosols in the ambient air of Gangotri Glacier valley of north-western Himalaya in India, Atmos. Environ., 214, 116879, https://doi.org/10.1016/j.atmosenv.2019.116879, 2019.

Pandey, C. P., Singh, J., Soni, V. K., and Singh, N.: Yearlong first measurements of black carbon in the western Indian Himalaya: Influences of meteorology and fire emissions, Atmos. Pollut. Res., 11, 1199–1210, https://doi.org/10.1016/j.apr.2020.04.015, 2020.

Prasad, P., Roja Raman, M., Venkat Ratnam, M., Chen, W.-N., Vijaya Bhaskara Rao, S., Gogoi, M. M., Kompalli, S. K., Sarat Kumar, K., and Suresh Babu, S.: Characterization of atmospheric black carbon over a semi-urban site of Southeast India: Local sources and long-range transport, Atmos. Res., 213, 411–421, https://doi.org/10.1016/j.atmosres.2018.06.024, 2018.

Romshoo, B., Bhat, M. A., and Habib, G.: Black carbon in contrasting environments in India: Temporal variability, source apportionment and radiative forcing, Atmos. Environ., 302, 119734, https://doi.org/10.1016/j.atmosenv.2023.119734, 2023.

Savadkoohi, M., Pandolfi, M., Reche, C., Niemi, J. V., Mooibroek, D., Titos, G., Green, D. C., Tremper, A. H., Hueglin, C., Liakakou, E., Mihalopoulos, N., Stavroulas, I., Artiñano, B., Coz, E., Alados-Arboledas, L., Beddows, D., Riffault, V., De Brito, J. F., Bastian, S., Baudic, A., Colombi, C., Costabile, F., Chazeau, B., Marchand, N., Gómez-Amo, J. L., Estellés, V., Matos, V., Van Der Gaag, E., Gille, G., Luoma, K., Manninen, H. E., Norman, M., Silvergren, S., Petit, J.-E., Putaud, J.-P., Rattigan, O. V., Timonen, H., Tuch, T., Merkel, M., Weinhold, K., Vratolis, S., Vasilescu, J., Favez, O., Harrison, R. M., Laj, P., Wiedensohler, A., Hopke, P. K., Petäjä, T., Alastuey, A., and Querol, X.: The variability of mass concentrations and source apportionment analysis of equivalent black carbon across urban Europe, Environ. Int., 178, 108081, https://doi.org/10.1016/j.envint.2023.108081, 2023.

Spohn, T. K., Martin, D., Geever, M., and O'Dowd, C.: Black carbon measurements from Ireland's Atmospheric Composition and Climate Change (AC3) network, Atmos. Environ., 271, 118932, https://doi.org/10.1016/j.atmosenv.2021.118932, 2022.

Sun, J., Birmili, W., Hermann, M., Tuch, T., Weinhold, K., Merkel, M., Rasch, F., Müller, T., Schladitz, A., Bastian, S., Löschau, G., Cyrys, J., Gu, J., Flentje, H., Briel, B., Asbach, C., Kaminski, H., Ries, L., Sohmer, R., Gerwig, H., Wirtz, K., Meinhardt, F., Schwerin, A., Bath, O., Ma, N., and Wiedensohler, A.: Decreasing trends of particle number and black carbon mass concentrations at 16 observational sites in Germany from 2009 to 2018, Atmos. Chem. Phys., 20, 7049–7068, https://doi.org/10.5194/acp-20-7049-2020, 2020.